# Phase-Field Modeling of Domain Structure of Confined Nanoferroelectrics

Julia Slutsker,[1,3,*] Andrei Artemev,[2] and Alexander Roytburd[3,†]

[1]*Ceramics Division, MSEL, NIST, Gaithersburg, Maryland 20899, USA*

[2]*Department of Mechanical and Aerospace Engineering, Carleton University, 1125 Colonel By Drive, Ottawa, Ontario K1S 5B6, Canada*

[3]*Department of Materials Science and Engineering, University of Maryland, College Park, Maryland 20742, USA*

(Received 29 May 2007; published 28 February 2008)

The results of phase-field simulation of domain structures (DSs) in ferroelectric nanorods of different shapes and sizes are presented. It is shown that equilibrium DSs consist of an electrostatically compatible circuit of 180° and 90° domains. A DS in a thin rod contains 90° cubic elastic domains. The trend to minimize the residual stress and the stray field results in the formation of crater-shaped sets of closed circuits of 90° domains, which can be mechanically incompatible but able to maintain electrostatic compatibility during the evolution under an applied electric field.

DOI: 10.1103/PhysRevLett.100.087602 PACS numbers: 77.80.Dj, 77.22.Ej, 77.84.Lf, 78.20.Bh

The interest in nanoferroelectrics has dramatically increased in the last decade [1,2]. While there are numerous theoretical studies of domain structures (DSs) in ferroelectric nanofilms, the DSs in confined nanoferroelectrics have not been studied yet, although there is experimental evidence of the domain existence in the nanorods that demonstrate piezoelectric response and polarization switching under an electric field [3,4]. In this Letter we use the phase-field modeling to predict DSs in ferroelectric nanorods.

An important insight into the DS of confined ferroelectrics has been provided by the first-principles-based simulations that have revealed a significant effect of the depolarizing field on dipole patterns in low dimensional ferroelectrics (rods, dots, etc.). It has been shown that the screening of a depolarizing field in confined ferroelectrics with the size of several nanometers proceeds through the alignment of polarization along the surfaces, resulting in the formation of vortex dipole patterns [5,6]. These results allow one to expect that with the increase in the size of ferroelectrics the vortex patterns transform to a closed circuit of 90° domains, thus minimizing the depolarizing field energy similarly to how closed flux domain configurations minimize the magnetostatic stray field energy in ferromagnetics. However, there is an important difference between DSs in ferroelectrics and ferromagnetics besides an obvious scale difference dictated by the different domain wall thickness. Since the spontaneous strain in ferroelectrics $(10^{-2} - 10^{-3})$ is much large than that in ferromagnetics $(10^{-4} - 10^{-5})$, the elastic interactions are strong in ferroelectrics and negligible in ferromagnetics. This leads to important peculiarities of DSs in confined ferroelectrics, as it is shown in this paper.

We present the phase-field (PF) simulation results of DSs in ferroelectric nanorods embedded into a nonferroelectric film clamped by a substrate. Similar nanostructures have been recently produced by the epitaxial self-assembling of ferroelectric and ferromagnetic phases on a single crystalline substrate [7–9], and their stress state and coupling properties have been studied by using analytical and PF modeling approaches [10–12].

The phase-field approach used in this study allows us to simulate the DS in the systems with a size up to 100 nm with different ratios between the strengths of electrostatic and elastic interactions, as well as to estimate different energy contributions to the thermodynamics of a DS system. In accordance with the PF approach, a DS is described as a distribution of polarization $P_i(r)$ or the order parameter $\eta_i(r)$, $P_i(\mathbf{r}) = P^0 \cdot \eta_i(\mathbf{r})$, where $P^0$ is the saturation polarization of a single domain equilibrium state. In order to model the DS in a periodic nanostructure with ferroelectric nanorods embedded into a nonpolarizing matrix we have simulated the evolution of the order parameter in the rods, while maintaining a fixed order parameter in the matrix. The equilibrium domain structure is described by the order parameter distribution corresponding to the minimum of the free energy functional $F = F_{\mathrm{GL}} + F_{\mathrm{electro}} + F_{\mathrm{el}}$, where $F_{\mathrm{GL}}$ is the Ginzburg-Landau potential, $F_{\mathrm{electro}}$ is the energy of electrostatic interactions, and $F_{\mathrm{el}}$ is the energy of elastic interactions.

The Ginzburg-Landau potential, $F_{\mathrm{GL}}$,

$$F_{\mathrm{GL}} = \int_V \left[ f_0(\eta_i) + \frac{1}{2}\beta_{ijkl}\frac{\partial \eta_i}{\partial x_k}\frac{\partial \eta_j}{\partial x_l}\right] dV, \qquad (1)$$

includes the homogeneous state energy density, $f_0(\eta_i)$, approximated by the Landau-Devonshire type expansion, and the energy of short-range interactions described by the gradient terms. For the three component order parameter, $\eta_i$, $i = 1, 2, 3$, $f_0$ is determined as

 

$$f_0(\eta_i) = \alpha_1(\eta_1^2 + \eta_2^2 + \eta_3^2) + \alpha_{11}(\eta_1^4 + \eta_2^4 + \eta_3^4) + \alpha_{12}(\eta_1^2\eta_2^2 + \eta_2^2\eta_3^2 + \eta_3^2\eta_1^2) + \alpha_{111}(\eta_1^6 + \eta_2^6 + \eta_3^6) + \alpha_{112}[\eta_1^2(\eta_2^4 + \eta_3^4) + \eta_2^2(\eta_1^4 + \eta_3^4) + \eta_3^2(\eta_1^4 + \eta_2^4)] + \alpha_{123}\eta_1^2\eta_2^2\eta_3^2. \quad (2)$$

This potential with the coefficients corresponding to the transformation from the cubic to tetragonal state in $PbTiO_3$ is used in the simulations. The second term in Eq. (2), wherein $\beta_{ijkl}$ is the gradient coefficient tensor, determines the interface energy. Since the value of the components of the gradient coefficient tensor $\beta_{ijkl}$ cannot be determined with a feasible accuracy due to the difficulties with the separation of short- and long-range interactions, in our simulations, we have used the isotropic gradient coefficient.

The electrostatic energy of the inhomogeneous distribution of polarization under an external field is used as introduced in [13,14]:

$$F_{dd} = \frac{1}{2\varepsilon_0\varepsilon^*}\int \frac{k_i k_j}{k^2}\{P_i(\mathbf{r})\}_{\mathbf{k}}\{P_j(\mathbf{r})\}^*_{\mathbf{k}}\frac{d^3k}{(2\pi)^3} - E_i\int_V P_i(\mathbf{r})dV, \quad (3)$$

where $\mathbf{k} = 0$ is excluded from the integration, symbol $\{\ldots\}_{\mathbf{k}}$ implies the Fourier transform, asterisk denotes a complex conjugate, $E_i$ is an external electric field, $\varepsilon_0$ is a dielectric constant of vacuum, and $\varepsilon^*$ is a high frequency dielectric constant not associated with the ferroelectric order parameter ($\varepsilon^*$ is in the order of 1 [6,15]). To emphasize the effect of electrostatic interactions we have assumed $\varepsilon^* = 1$. The first term in Eq. (3) is an equivalent to $-1/2\int_V E_{\text{int}}PdV$, where $E_{\text{int}}$ is an internal electrostatic field and describes the energy of electrostatic interactions between inhomogeneities in the polarization distribution without the Lorentz field energy. The Lorentz field energy is included in the Landau-Devonshire free energy [Eq. (2)]. Thus, Eq. (3) incorporates long-range electrostatic interactions within the phenomenological Landau theory [13,16].

The energy of long-range elastic interactions is determined as

$$F_{\text{el}} = \int_V\left[\frac{1}{2}C_{ijkl}[\varepsilon_{ij}(\mathbf{r}) - \varepsilon^0_{ij}(\mathbf{r})][\varepsilon_{kl}(\mathbf{r}) - \varepsilon^0_{kl}(\mathbf{r})]dV\right] - \sigma^{\text{appl}}_{ij}\int_V \varepsilon^0_{ij}(\mathbf{r})dV, \quad (4)$$

where $C_{ijkl}$ is the elastic modulus, $\varepsilon_{ij}(\mathbf{r})$ is the total strain, and $\sigma^{\text{appl}}_{ij}$ is an external stress. The transformation self-strain $\varepsilon^0_{ij}(\mathbf{r}) = Q_{ijkl}P_i(\mathbf{r})P_k(\mathbf{r})$, where $Q_{ijkl}$ is an electrostrictive coefficient tensor. The elastic moduli are assumed to be equal in the rod and matrix.

The equilibrium field of the order parameters $\eta^0_i(\mathbf{r})$ is a solution of the equation $\delta F/\delta\eta_i(\mathbf{r}) = 0$, which is obtained by solving the time-dependent Ginzburg-Landau equation using a fast Fourier transform method [13]:

$$\frac{\partial\eta_i}{\partial t} = -L\frac{\delta F}{\delta\eta_i} + \xi_i, \quad (5)$$

where $L$ is the kinetic coefficient and $\xi_i$ is the Langevin noise term. According to the microelasticity approach in the PF modeling [13,17], the evolution of the microstructure is described by the solution of Eq. (5) presented in the reciprocal space.

The following dimensionless parameters have been used in the simulations: (a) dimensionless Landau coefficients, $\alpha/\Delta f$, where $\Delta f$ is the difference between the energies of equilibrium paraelectric ($\eta_i = 0$) and ferroelectric states ($\eta_i = \eta^0_i$), where $\partial f_0(\eta_i)/\partial\eta_i = 0$; (b) dimensionless gradient coefficient $\tilde{\beta} = \beta/\Delta f l_0^2$, where $l_0$ is the computation grid length that determines the calculation length scale, $l_0 = l\beta^{-1/2}$, where $l$ is the thickness of ferroelectric domain walls ($l \sim 1$ nm); (c) characteristic elastic energy, $\zeta = \bar{\varepsilon}^0_{ij}C_{ijkl}\bar{\varepsilon}^0_{kl}/(2\Delta f)$, where $\bar{\varepsilon}^0_{ij} = Q_{ijkl}P^0_iP^0_k$; (d) characteristic energy of electrostatic interactions, $\lambda = P^{02}/(2\pi\varepsilon_0\Delta f)$.

A $512 \times 64 \times 64$ mesh with periodic boundary conditions has been used for the simulation of a rod surrounded by a dielectric matrix (a symmetrical cell). The electrostatic image charge principle has been used so that a half of this cell, $256 \times 64 \times 64$, represented the rod with one of its ends covered by an electrode (an asymmetrical cell). The transformation from an unstable paraelectric occurs through the nucleation of a stable ferroelectric phase driven by the Langevin noise in the evolution Eqs. (5). After a sufficiently long relaxation process the equilibrium is established between all domains, and in the final part of the simulation process the domain pattern remains stationary.

DSs have been investigated in confined ferroelectric nanorods with different cross section shapes and sizes. To reveal relative effects of electrostatic and elastic energies two different $\lambda/\zeta$ ratios have been used in the simulations: $\lambda/\zeta = 25$, corresponding to ferroelectrics with a large spontaneous deformation, such as $PbTiO_3$ or $BaTiO_3$ at room temperature, and $\lambda/\zeta = 250$, corresponding to ferroelectrics with a small spontaneous deformation. A similar increase in the value of $\lambda/\zeta$ can be the result of the decreasing saturation polarization in ferroelectrics with an increasing temperature.

Figure 1 presents the DS in a rod oriented along $\langle 100\rangle$ with a square cross section and $\{100\}$ faces. The modeling has been performed with $\tilde{\beta} = 8$, corresponding to the cross section length of 16 nm, and with the ratio of elastic to electrostatic energies, $\lambda/\zeta$, equal to 25. The DS consists of closed circuits of 90° and 180° domains [Fig. 1(a)]. The 90° domains have different functions in different parts of the rod. While the triangle prismatic domain at the end of the rod screens the electrostatic stray field, the cubic domains in the middle of the rod decrease elastic energy caused by the rod/matrix misfit. The cubic domains cannot

eliminate the internal stresses completely because (1) they do not affect the misfit strain normal to the plane of polarization, and (2) their formation is accompanied by the disclination-type distortion [Fig. 1(b)]. Taking into account that the relaxation through the formation of 90° domains is possible only if the relaxed elastic energy is larger than the interface domain energy, one may expect that the cubic domains do not appear in DSs if the elastic energy decreases. Indeed, DSs obtained at $\lambda/\zeta = 250$ and $\tilde{\beta} = 8$ [Fig. 1(c)] do not contain cubic 90° domains. These observations as well as the disappearance of the cubic domains under the external compression applied along the rod allow us to conclude that 90° cubic domains in constrained nanorods are elastic domains [18]. It should be emphasized that the DS presented above is an equilibrium one: it can be removed by an applied electric field and then reappear after the field has decreased. The electrostatic compatibility (the zero charge on the domain interfaces) is maintained during the domain evolution under an electric field [Fig. 1(d)]. It makes this evolution continuous and the DS changes reversible.

A high level of residual stresses in simple DSs discussed above makes them less thermodynamically preferable than more complex structures in the rods with a larger thickness, where the larger part of the elastic energy can relax despite the increase in the interface energy. We present an example of the results of the simulations of the DS at $\lambda/\zeta = 25$ and $\tilde{\beta} = 2$, corresponding to the cross section thickness of 35 nm. In this case a crater-shaped closed circuit configuration of four 90° domains with complete screening of electrostatic stray field at the end of the rod is formed.

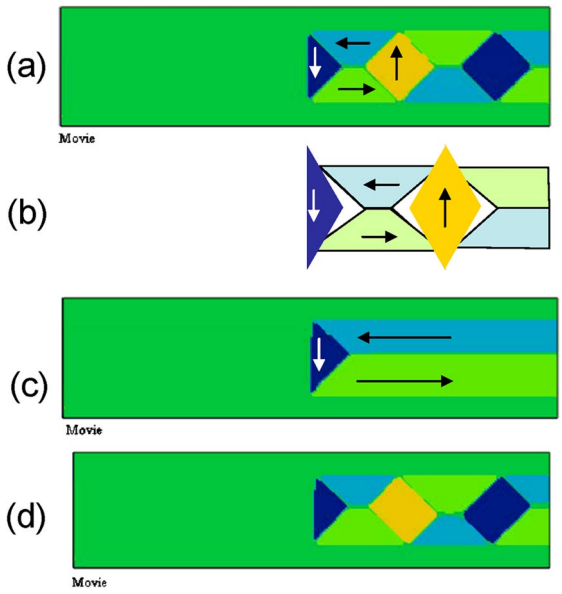


FIG. 1 (color online). A longitudinal view of the DS in square-shaped rods with the cross section length of 16 nm (a half of the computational cell is shown). Domain boundaries are normal to the picture plane. (a) DS at $\lambda/\xi = 25$. (b) Disclination distortion due to the 90° domain formation. (c) DS at $\lambda/\xi = 250$. (d) DS under the electric field.

The relaxation of the misfit stress inside the rod proceeds through the formation of a complex hierarchical structure including 90° stripe domains. An irregular structure inside the middle of the rod is eliminated by the electric field and does not return when the field is removed. As a result, a metastable DS is obtained, which consists of the crater-shaped 90° domain assembly at the end of the rod and a cylindrical configuration of 180° domains [Fig. 2(a)]. The 90° and 180° DSs are connected through a system of 90° domain walls oriented along {111} planes [Fig. 2(b)]. The condition for the electroneutral domain boundary, $\Delta\mathbf{P} \cdot \mathbf{n} = 0$, leaves one of the $\mathbf{n}$ components free and, therefore, allows for the {111} oriented domain boundaries without charges. These DSs maintain the electrostatic compatibility during the electric field induced evolution and, therefore, change reversibly under the ac field. The equilibrium state of the rod corresponds to a "bamboo" structure [presented schematically in Fig. 2(c)] with a periodical alternation of the 180° domains and double-crater-shaped sets of 90° domains similar to those at the end of the rod. However, this complex equilibrium structure could not be reached within a reasonable simulation time. With a decreasing contribution of the elastic energy, $\lambda/\zeta = 250$, the DS is similar to the simplest one present in Fig. 1(c).

The DSs in nanorods with circular cross sections of different diameters are presented in Fig. 3. The DS in a nanorod at $\tilde{\beta} = 8$, corresponding to the diameter of 16 nm and with $\lambda/\zeta = 25$, is similar to the one obtained in the square rod [Fig. 1(a)]. However, the domain walls between 90° domains have a cylindrical shape [Fig. 3(a)]. Although there are no electrical charges on these curved domain walls, they are the sources of internal stresses. Their presence in an equilibrium DS is dictated by the shape of rods

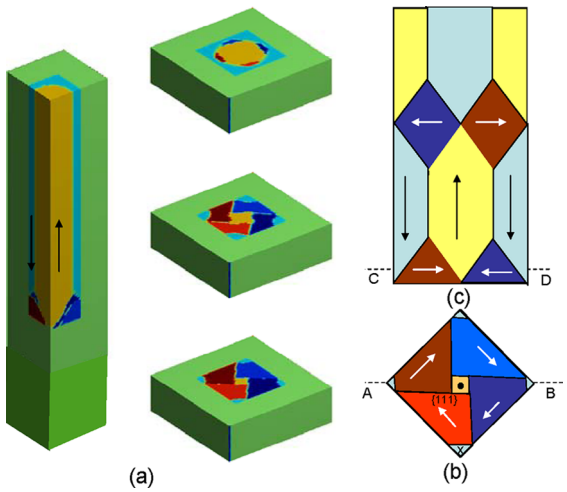


FIG. 2 (color online). DS in a square-shaped rod with the cross section length of 35 nm. (a) Series of plane cross sections along the ferroelectric rod, from the end of the rod (bottom) toward the middle of the rod (top). (b) A schematic of the domain wall arrangement in the section along CD plane [Fig. 2(c)]. (c) Equilibrium DS at $\lambda/\xi = 25$, the section along AB plane [Fig. 2(b)] is shown.

and is a result of a relatively small effect of the elastic energy in comparison to the electrostatic energy of the depolarizing field.

Contrary to the DS in a square rod, the simple DS above is not able to completely remove the stray electrostatic fields. Therefore the complexity of the DS in circular shaped nanorods increases with the increase in the diameter, even if the effect of the elastic stress is negligible. Figure 3(b) presents the DS in a nanorod with $\tilde{\beta} = 2$, corresponding to the diameter of 35 nm and with $\lambda/\zeta = 250$. The stray field at the end of the rod is compensated by the formation of the closed circuit configuration consisting of four 90° domains with domain walls oriented along {111}. The cylindrical 180° axial domains are formed far from the end of the rod. A closed circuit of 90° domains is connected with an outer axial domain along the {111} domain walls and with an inner axial domain along the distorted {110} domain walls [Fig. 3(c)]. These distorted {110} plane walls as well as the curved 90° domain walls in Fig. 3(a) appear due to the effect of the depolarizing field of the nanorod cylindrical surface.

The structures presented in this paper are expected to be found in confined ferroelectrics where the effect of electrostatic interactions, particularly of the depolarizing field, is not diminished by the screening free charges. Therefore, these DSs could not be observed in the experiments with nanorods attached to a conductive substrate [3,4]. The principal specific feature of DSs in nanorods is the compatible configurations of 180° and 90° domains. The 90° domains minimize electrostatic energy of the depolarizing field as well as elastic energy due to the mechanical constraint. The dominant effect of the electrostatic interactions

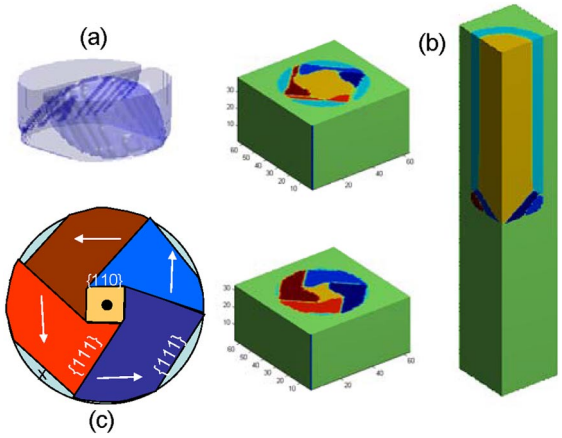


FIG. 3 (color online). DS in a circular shaped rod (a) Domain boundaries of 90° domains inside the rod with the diameter of 16 nm and $\lambda/\xi = 25$. (b) Series of plane sections along the circular shaped rod with the diameter of 35 nm and $\lambda/\xi = 250$. Sections show the DS from near the end of the rod (bottom) toward the middle of the rod (top). (c) A schematic of the domain wall arrangement.

can cause the formation of nonconventional 90° domain walls, which do not satisfy the condition of strain compatibility. These domain walls are charge-free, but they can have an unusual orientation or be curved. In constrained nanorods the closing 90° domains minimize the electrostatic energy of stray fields while the inner 90° domains minimize the elastic energy (cubic domains in thin nanorods). The elastic 90° domains obviously should not develop in unconstrained rods that should have the DSs presented in Figs. 1(c), 2(a), and 3(b). On the other hand, the trend to minimize the energy of the elastic interaction between domains results in the formation of a multidomain crater-shaped 90° domain configuration, which decreases the energy of the residual stress while not violating the electrostatic compatibility between 90° and 180° domains. The equilibrium DSs are able to maintain the electrostatic compatibility between domains during their change under the electric field, thus making possible a continuous evolution of the structure under the electric field.

A. A. gratefully acknowledges the support of NSERC. A. R. is grateful to the financial support of NSF and Israel-USA Binational Science Foundation.

*julias@nist.gov
†roytburd@wam.umd.edu

[1] J. F. Scott, Science **315**, 954 (2007).
[2] M. Alexe and D. Hesse, J. Mater. Sci. **41**, 1 (2006).
[3] G. Suyal *et al.*, Nano Lett. **4**, 1339 (2004).
[4] J. Wang *et al.*, Appl. Phys. Lett. **90**, 133107 (2007).
[5] I. V. Naumov, L. Bellaiche, and H. Fu, Nature (London) **432**, 737 (2004).
[6] S. Prosandeev and L. Bellaiche, Phys. Rev. B **75**, 094102 (2007).
[7] H. Zheng *et al.*, Science **303**, 661 (2004).
[8] J. Slutsker *et al.*, Phys. Rev. B **73**, 184127 (2006).
[9] I. Levin *et al.*, Adv. Mater. **18**, 2044 (2006).
[10] J. Slutsker *et al.*, J. Mater. Res. **22**, 2087 (2007).
[11] J. Slutsker and A. L. Roytburd, Phase Transit. **79**, 1083 (2006).
[12] J. X. Zhang *et al.*, Appl. Phys. Lett. **90**, 052909 (2007).
[13] A. G. Khachaturyan, *Theory of Structural Transformations in Solids* (John Wiley & Sons, New York, 1983).
[14] S. Semenovskaya and A. G. Khachaturyan, Ferroelectrics **206–207**, 157 (1998).
[15] J. Hlinka and P. Marton, Phys. Rev. B **74**, 104104 (2006).
[16] L. D. Landau and E. M. Lifshitz, *Electrodynamics of Continuous Media* (Pergamon Press, New York, 1986), Vol. 8, 2nd ed.
[17] A. Artemev, Y. Wang, and A. G. Khachaturyan, Acta Mater. **48**, 2503 (2000).
[18] The formation of vortices inside the rods with the thickness of several nanometers obtained by the first-principles-based simulations [5,6] is likely a result of the constraint effect of the free surface of very thin rods.